Magnetization dynamics of buckling domain structures in patterned thin films

C. Patschureck,[1,2,*] K. Lenz,[3] M. O. Liedke,[3] M. U. Lutz,[4] T. Strache,[3,†] I. Mönch,[5] R. Schäfer,[1,2] L. Schultz,[1,2] and J. McCord[6]

[1]*Institute for Metallic Materials, IFW Dresden, P.O. Box 270116, 01171 Dresden, Germany*

[2]*Department of Mechanical Engineering, Institute for Materials Science, TU Dresden, 01062 Dresden, Germany*

[3]*Institute of Ion Beam Physics and Materials Research, Helmholtz-Zentrum Dresden-Rossendorf, P.O. Box 510119, 01314 Dresden, Germany*

[4]*Institute for Solid State Research, IFW Dresden, P.O. Box 270116, 01171 Dresden, Germany*

[5]*Institute for Integrative Nanosciences, IFW Dresden, P.O. Box 270116, 01171 Dresden, Germany*

[6]*Institute for Materials Science, CAU Kiel, Kaiserstrasse 2, 24143 Kiel, Germany*

(Received 22 May 2012; published 17 August 2012)

The magnetodynamics of lens-shaped thin-film elements are studied using vector network analyzer ferromagnetic resonance. A strong increase in the frequency at resonance is found when approaching the switching field. From magnetic force microscopy imaging the increase in resonance frequency is ascribed to the formation and evolution of a buckling domain state. The experimental data are qualitatively reproduced by micromagnetic simulations of a model element. Thereby, the roles of the external magnetic field and the buckling wavelength are extracted separately. Magnetic domain modes with dynamic magnetization modulations parallel and perpendicular to the static magnetization are identified. Based on magnetostatic energy considerations qualitative arguments are derived that allow for an interpretation of the dynamic response in such low-symmetry magnetization distributions.

DOI: 10.1103/PhysRevB.86.054426 PACS number(s): 75.78.Fg, 75.70.Kw, 76.50.+g, 68.37.Rt

I. INTRODUCTION

The dynamic magnetization response of magnetically saturated films and micrometer- or nanometer-size elements has been extensively studied in recent years.[1–9] In the simplest case a uniform precessional motion of the magnetization vector is observed. The uniform resonance is described by Kittel's equation[1] for $H_{\mathrm{eff}} \ll M_{\mathrm{s}}$,

$$f_{\mathrm{r}}^2 = \left(\frac{\gamma \mu_0}{2\pi}\right)^2 M_{\mathrm{s}} H_{\mathrm{eff}}, \tag{1}$$

with the gyromagnetic ratio $\gamma = 1.76 \times 10^{11}$ T^{-1} s^{-1}, the vacuum permeability $\mu_0 = 4\pi \times 10^{-7}$ Vs/Am, the saturation magnetization M_s, and the effective field H_{eff}. In addition to uniform resonance, a variety of modes, which are dominated by dipolar or exchange fields, have been identified.[2,7,9] Localized modes are often observed due to a strong inhomogeneity of the demagnetizing field (see, e.g., Refs. 4, 5, and 10). The dynamic response of nonsaturated films and elements, on the other hand, is strongly determined by the presence of magnetization inhomogeneities and domain walls. The first dynamic experiments on nonsaturated ferrite films performed by Polder and Smit[11] back in the 1950s promoted numerous studies on the resonance phenomena in stripe domain structures.[12–15] Since then, also the dynamic behavior of films with *in-plane* anisotropy and highly symmetric domain configurations has gained a lot of interest, e.g., magnetic dots in the vortex state or square elements with a Landau domain structure.[16–21] So far, strongly confined modes that are localized in the domain volume, at the vortex center, or at the domain walls have been identified and studied both experimentally and numerically. Higher order domain and wall modes have been found, similar to spin-wave modes observed in saturated films. Bailleul *et al.*[21] elaborately discussed the role of domain walls on the localization and quantization of spin-wave modes in a Landau domain state. In element geometries and domain structures of low symmetry a large set of modes might be excited instead of a few individual quantized modes due to a rather complex dipole-exchange dispersion.

For the purpose of understanding the dynamics in complex magnetic domain configurations, here we present absorption measurements on concertina or buckling domain patterns at different magnetic fields. Concertina patterns may be observed in soft ferromagnetic thin-film structures close to zero magnetic field after saturation along the hard axis.[22–24] However, such domain configurations often tend to collapse by the nucleation and propagation of Blochlines that may be triggered by small magnetic-field variations. In lens-shaped elements the buckling domain state was found to be stable over a wide magnetic-field range.[25] Therefore, we first performed static and dynamic measurements on elongated lens-shaped structures. Associated with the reversal process we found a significant increase in the main resonance frequency at magnetic fields smaller than the switching field. This behavior strongly differs from the frequency dispersion that accompanies the switching process of extended films, exchanged biased systems,[26] or ring structures[27] or the behavior of the gyrotropic vortex mode in magnetic disks.[28] In all these examples, a decrease in the precessional frequency with an increase in the applied field amplitude (negative dispersion) is found until the structures switch into the new field direction. In the second step, we simulated the dynamic response of a model stripe to gain further understanding of the experimentally observed resonance features, as well as their dependence on the externally applied magnetic field and the buckling wavelength. In the last section we derive qualitative arguments to explain the dynamic domain modes based on dynamic magnetic charge considerations.

II. EXPERIMENTS

A ferromagnetic thin film of amorphous $Co_{40}Fe_{40}B_{20}$ with a thickness of 60 nm was prepared on a glass wafer by means of ultrahigh-vacuum magnetron sputtering at room temperature.

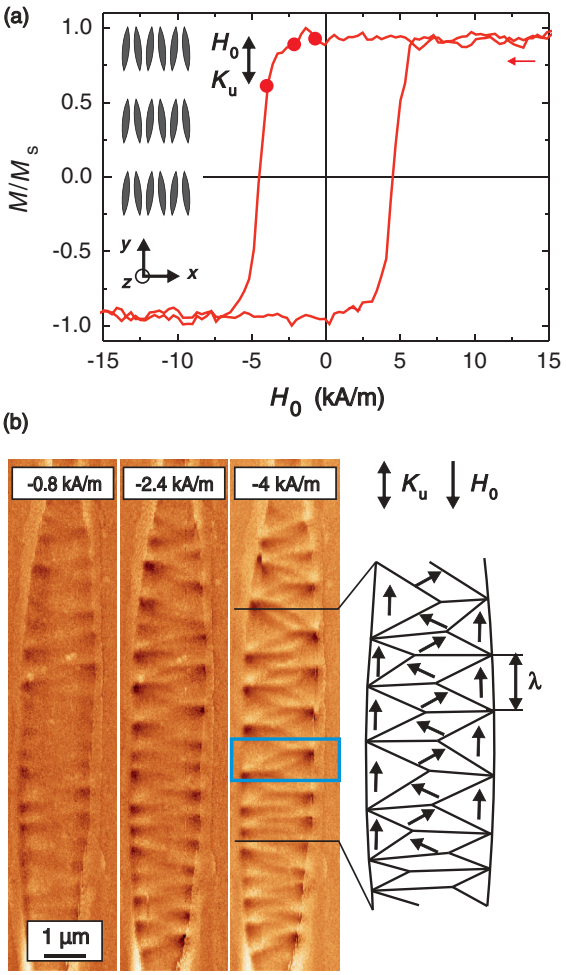

FIG. 1. (Color online) (a) Normalized magneto-optical magnetization curve measured in magnetic fields H_0 applied along the easy axis ($K_u \| y$ axis) of lens structures (see inset) and (b) MFM measurements corresponding to magnetic fields indicated in (a) by filled (red) circles. The (blue) rectangle highlights the area where coarsening of the domain pattern occurred after increasing the reversal-field amplitude to -4 kA/m. The sketch illustrates the magnetization configuration in the buckling domain pattern and indicates the wavelength λ.

To induce a uniaxial anisotropy, an in-plane magnetic field of $H_{\mathrm{dep}} = 20$ kA/m was applied during film deposition. An array of lens-shaped structures with element dimensions of $2 \times 20\ \mu\mathrm{m}^2$ [see inset in Fig. 1(a)], with the long axis being parallel to the induced anisotropy axis, was structured using photolithography. The lateral spacing between individual element rows was chosen to be equal to the element dimensions to reduce effects originating from magnetostatic interaction. The whole array comprised 1350×230 lens-shaped thin-film structures. A saturation magnetization of $\mu_0 M_s = 1.48$ T was extracted from out-of-plane magnetization curve measurements of an unpatterned reference film (not shown). In-plane magneto-optical hysteresis measurements along the magnetic hard axis of the reference film (not shown) yielded a uniaxial anisotropy field of $H_a = 1.6$ kA/m. A magnetization loop along the magnetic easy axis of the patterned structures [displayed in Fig. 1(a)] reveals a coercive field H_c of 4.4 kA/m.

A. Magnetic domain observation

Domain studies have been performed by magnetic force microscopy (MFM), working with a commercial low-moment magnetic tip in the tapping mode. Thereby, the cantilever deflection is detected as a measure of the interaction strength between the stray field of the tip and the stray field above the sample surface generated by magnetic charges in the sample.[23,29] For an in-plane magnetized thin-film structure, *magnetic charges* may emerge at the structure edges if $\mu_0 \vec{M}_s \cdot \vec{n} \neq 0$, with n being the surface normal. Additionally, dipolar magnetic volume charges are distributed in the tails of magnetic Néel domain walls.[23] In order to prevent the tip magnetization to be switched by strong stray fields emerging from the lens tips, only the inner region of the lenses was scanned. Figure 1(b) shows MFM pictures of a representative lens obtained at different magnetic fields. The field was applied opposite to the previous saturation direction.

Note that the contrast in the MFM images is caused by a superposition of stray fields emerging at the element edges due to roughness and volume charges located at the domain walls.[30] When the external magnetic field parallel to K_u is reduced from positive saturation to 0, a zigzag-like canting of the magnetization is first observed (not shown), which then transforms into a buckled domain pattern when the field direction is reversed.[25] The sketch in Fig. 1(b) qualitatively illustrates the position of the domain walls and the magnetization distribution in the buckling structure at a field of -4 kA/m. The magnetization of the volume domains is canted with respect to the easy axis, whereas the edge domain magnetization remains parallel to the edges along the former saturation direction to avoid magnetic surface charges. Neither domain wall dragging nor any other irreversible change of the domain structure due to the tip stray field was observed during several scans at a constant magnetic field. Increasing the field amplitude leads to a stronger domain wall contrast, which we interpret as an increasing domain wall angle and hence a stronger diploar charging of the walls due to a stronger magnetization canting in neighbored volume domains. Despite an increase in the field the wavelength λ of the buckling pattern was found to be mainly constant (for $H_0 > -H_c$). Only in distinct areas [see (blue) rectangle in the lens center] had some coarsening occurred. At $H_0 = -H_c$ the buckling pattern breaks down and the magnetization switches to the field direction.

B. Ferromagnetic resonance

Knowing the domain structure, vector network analyzer ferromagnetic resonance (VNA-FMR)[31] experiments were carried out to study the corresponding dynamic response. Thereby the self-inductance of a coplanar waveguide (width: 200 μm), loaded with an upside-down-oriented sample, is measured for a wide range of frequencies of sinusoidal excitation. A high magnetic field reference measurement is subtracted from all measurements to get the pure magnetic response. Any resonance phenomenon in the sample causes a change in the self-inductance of the waveguide, resulting in a dip in the microwave transmission parameter $|S_{21}|$. Frequency sweeps were performed at various bias fields H_0, starting with the sample being magnetized along a positive saturation field

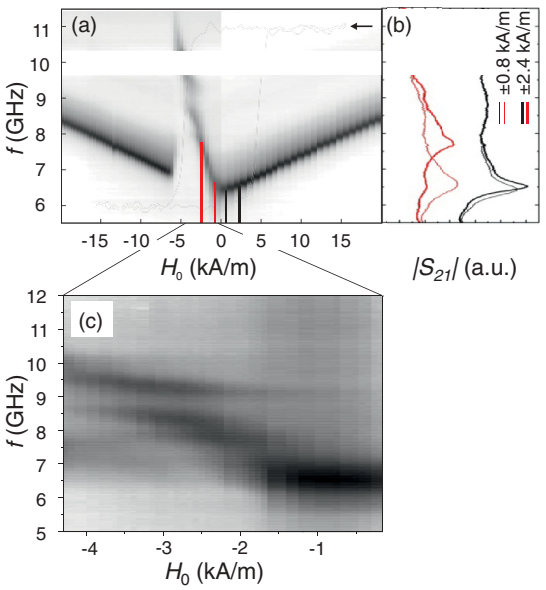

FIG. 2. (Color online) (a) FMR signal of lens structures measured over a wide magnetic field range starting at positive saturation as indicated by the black arrow. The field sweep corresponds to the demagnetizing branch of the hysteresis curve. Dark colors in the spectrum represent dips in the amplitude of the microwave transmission parameter $|S_{21}|$ that is shown for selected field values in (b). The thin and thick solid curves correspond to negative (red) and positive (black) bias field values of 0.8 and 2.4 kA/m, respectively. Whereas the $f(H_0)$ dispersion follows the Kittel relation for $H_0 > 0$ and $H_0 < -H_c$, a much more pronounced shift of the resonance dip position towards higher frequencies is observed in the low negative field range. In a frequency range between 9.7 and 10.3 GHz we have masked a strong impedance change with a white bar. This artifact was observed in all measurements and could be attributed to disturbing reflections in the waveguide. As shown in (c), multiple resonance modes are resolved for $H_c < H_0 < 0$ in addition to the stronger resonance increase.

(with the H_0|| lens axis). Subsequently, the field was reduced to 0 and an increasing negative H_0 was applied. Consequently, the field sweep followed the demagnetizing branch of the hysteresis curve as indicated in Fig. 2(a). The intensity plot in Fig. 2(a) illustrates the resonance behavior over a wide range of H_0. Dark colors represent the minima of the microwave transmission parameter and indicate resonance in the sample. The graph in Fig. 2(b) shows $|S_{21}|$ for two selected bias-field values in the negative [left (red) curves] and positive [right (black) curves] magnetic-field range.

To interpret the data, let us start with the simple case where the positive bias field is strong enough to align the magnetization with the field. Decreasing the bias field results in a decrease in the effective field in the sample and thus in a shift of the resonance dip to a lower frequency according to Eq. (1), where $f \propto \sqrt{H_0 + H_k}$. Here, the effective anisotropy H_k represents the sum of the induced anisotropy H_a and the shape anisotropy contribution. When the field is then increased in the opposite direction with respect to the former saturation, the resonance frequency follows a positive dispersion. For -5 kA/m $< H_0 < 0$ the frequency increase with bias field is significantly enhanced [Fig. 2(a)] compared to the Kittel behavior observed in the positive field range. As shown more clearly in the finer-resolved FMR spectra in Fig. 2(c), the dynamic spectrum exhibits several distinct modes in the considered field range. The dip in the measurement curves [see left (red) curves in Fig. 2(b)] is much broader compared to the positive field regime, especially for small $|H_0|$. In addition to this main absorption peak, we observed a broad resonance feature of low amplitude for $-H_c < H_0 < 0$ (not shown). It appears obvious that these effects are related to the formation of the buckled domain structure and changes in the domain state with increasing field amplitude. This assumption manifests itself when reaching the switching field at ≈ -5 kA/m, where the resonance frequency drops to the uniform mode frequency as the magnetization has aligned parallel to the direction of the applied field. By driving minor loops of H_0 (not shown), with $H_0 > -H_c$, we could prove the reversibility of the dynamic spectra. Consequently, the spectrum is not influenced by irreversible changes in the magnetic domain structure.

The observed resonance behavior at magnetic fields -5 kA/m $< H_0 < 0$ differs remarkably from the negative dispersion which was expected for this field range.[5,26,28] To allow for an interpretation of the observed resonance behavior in the domain regime, the dynamic magnetization response of a model system is simulated using the object-oriented micromagnetic framework (OOMMF).[32]

III. MICROMAGNETIC SIMULATION

Using the dimensions of the experimentally investigated lens structures in any numeric micromagnetic simulation is challenging due to the huge computational time. Hence, for a qualitative comparison a rectangular model stripe with dimensions of $L_x = 1.5$ μm, $L_y = 4$ μm, and $L_z = 60$ nm, discretized in $(5 \times 5 \times 60)$–nm^3 cells, was chosen, as the buckling pattern is expected to emerge in such a structure too. In addition, periodic boundary conditions[34] were applied along y to promote the formation of a buckling pattern rather than a closure domain state. To compensate for the large shape anisotropy due to the periodic boundary conditions and to stabilize the domain pattern, a relatively large uniaxial anisotropy with $K_u = 2950$ J m^{-3} was set parallel to the x axis. The exchange constant, saturation magnetization, and damping constant were set to $A = 28.4 \times 10^{-12}$ J/m,[33] $\mu_0 M_s = 1.48$ T, and $\alpha = 0.005$, respectively, in agreement with static and dynamic measurements in unpatterned reference films. Domain patterns that form within the convergence criterion of $\delta m/\delta t = 1 \times 10^{-8}$ are regarded as metastable, low-energy configurations that are, in the second step, excited by a pulse magnetic field of $\mu_0 H_x = 0.5$ mT with a rise time of 6 ps and a Boltzmann shape. Such a pulse shape was proven to cover the excitation frequency range of interest, whereby the chosen pulse amplitude was regarded to be low enough to avoid fundamental changes in the domain structure. The out-of-plane susceptibility is proportional to the Fourier transform of the precessing magnetization component $M_z(t)$.

For the simulation, the initial magnetization was set along y. For a positive field of $\mu_0 H_y = 19.4$ mT the stripe is saturated along y and the fast Fourier transform amplitude spectrum in Fig. 3(a) (top) shows one pronounced peak at 9.4 GHz.

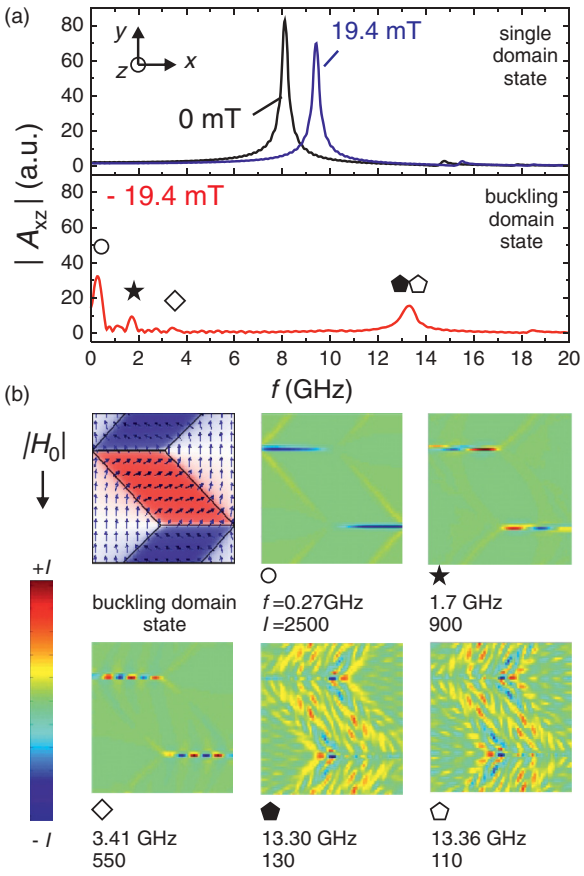

FIG. 3. (Color online) (a) Amplitude spectra of a homogeneously magnetized stripe at $H_y = 19.4$ and 0 mT (top) and of a stripe in a reversed field of $H_y = -19.4$ mT (bottom), excited by a pulse field along x. (b) The magnetization configuration (top row, left) shows a repetition unit of the buckling pattern at $H_y = -19.4$ mT. Spatial dynamic mode profiles correspond to the resonance features marked in the amplitude spectrum. The color maps for the different frequencies are scaled with respect to the corresponding maximum intensity $|I| = |A_i \cos(\phi_i)|$.

This intense resonance feature corresponds to the uniform precessional mode. The broadness of the peak reflects the fact that the demagnetizing field perpendicular to the stripe axis is not homogeneous. After reducing the field to 0, the stripe remains saturated along the stripe axis due to the strong shape anisotropy. In accordance with the Kittel equation, the frequency of the uniform mode is reduced to 8.1 GHz at zero field. The small peak that appears at a frequency of 14.4 GHz originates from the excitation of a higher order quantized mode with two nodes. Increasing the field in the opposite direction with respect to the former saturation leads to the formation of a buckling pattern until the reversed field is strong enough to switch the magnetization towards the new field direction. The wavelength λ of the buckling state strongly depends on the chosen L_y due to the fact that the stripe length represents a repetition unit in the periodic boundary condition calculation. Furthermore, coarsening of the simulated buckling pattern occurs when increasing the reversal field. For this reason the ratio of buckling wavelength to stripe width is higher in the simulation compared to the experiment. This artifact can be tolerated for our purposes, as we do not intend to give a quantitative reproduction of the presented measurement data. Here we, rather, want to gain a *qualitative* understanding on how the domain evolution affects the magnetization dynamics at different applied fields. The role of the buckling wavelength is discussed in Sec. III B by comparing the dynamic properties of a coarse and a fine buckling pattern at a constant magnetic field. Figure 3(a) (bottom) shows the amplitude spectrum calculated for the buckling pattern at $\mu_0 H_y = -19.4$ mT. Instead of a single resonance peak, multiple broad resonance features appear. An intense peak shows up at 13.3 GHz, which is much higher than the resonance frequency of the uniform mode. Several additional peaks appear in the low-frequency part of the spectrum.

To identify the different resonance modes, the precessional amplitude $A_i(f)$ and phase $\phi_i(f)$ in each cell i were determined for several frequencies via Fourier transformation of the local precessional motion $M_z(i,t)$. The spatial profiles of the resonance modes are found by extracting $I = A_i \cos(\phi_i)$ for the peak frequencies.[19] To save computation time, the dynamic response of every fifth cell (in the x and y direction) was analyzed, which has been proven to be fine enough to resolve all relevant mode features. Snapshot representations of the magnetic precessional motion [shown in Fig. 3(b)] reveal the relative out-of-plane magnetization amplitudes, where red and blue areas represent dynamic magnetization components pointing out of or into the film plane, respectively. Clearly, the first three peaks in the low-frequency range correspond to modes whose amplitudes are localized at the domain walls. Wall modes with zero, two, and five nodes are identified, for which the mode frequency increases with increasing nodal number. In contrast, the amplitude of the high-frequency peak is spread over the entire domain area. The width of the peaks can be explained by an overlap of the susceptibility of similar modes whose frequency spacing is too small to be resolved (compare, e.g., mode images for 13.3 and 13.36 GHz). In contrast to the dynamic response of saturated highly symmetric elements, no individual well-resolved modes are observed in irregularly shaped elements with inhomogeneous magnetization patterns.[21] Analyzing the snapshot representations of the domain mode profile in more detail, it is obvious that no uniform dynamic response is excited. Instead, the phase-corrected amplitude $A_i \cos(\phi_i)$ varies along and perpendicular to the magnetization direction inside the individual domains. Thereby, the mode profiles clearly reflect the position of domain walls in the underlying domain structure as well as the change in the magnetization direction from the closure to the basic domains. Comparing the local magnetization amplitudes with the color scale bar reveals that there is a net dynamic magnetization deflection out of the film plane because the deflection is positive over almost the entire domain area.

Note that a discretization of the simulation volume along the thickness would presumably result in further modes. We restricted the simulations to the two-dimensional case, as the results reflect the measurement data sufficiently well. Possible modes with an amplitude modulation along the film thickness of 60 nm are expected to exhibit much higher frequencies due to a strong exchange energy contribution.

In the following we concentrate on the discussion of the high-frequency domain mode, as it lies in the frequency range

of the main dynamic response in our experimental measurements. To understand the origin of the drastic resonance frequency increase that goes along with the formation of the domain pattern in our experiments, let us now study the dynamic response of the buckling pattern at varying external field strengths.

A. Effect of static magnetic field

In order to elude changes in the buckling wavelength in the first step, the coarsened domain state that was found just before switching [at $H_0 = -19.4$ mT; see Fig. 3(b)] was taken as the initial state. To study the effect of different applied magnetic-field amplitudes we then traced back the hysteresis branch to negative fields of -15 and -14 mT. Hence, a refining of the coarse initial pattern does not occur since the formation of additional domain walls would require the overcoming of an energy barrier. In accordance with our experimental observations (Sec. II A), the magnetization of the basic domains gradually tilts back towards the easy axis when reducing the applied negative field. The angle of the diagonal domain walls and the length of the horizontal walls adapt to these changes in order to avoid magnetic charges at the walls [compare magnetization details in Fig. 4(b)].

Figure 4 compares the dynamic response of a buckling pattern with a constant wavelength at different negative magnetic fields. The frequencies of similar domain wall modes are

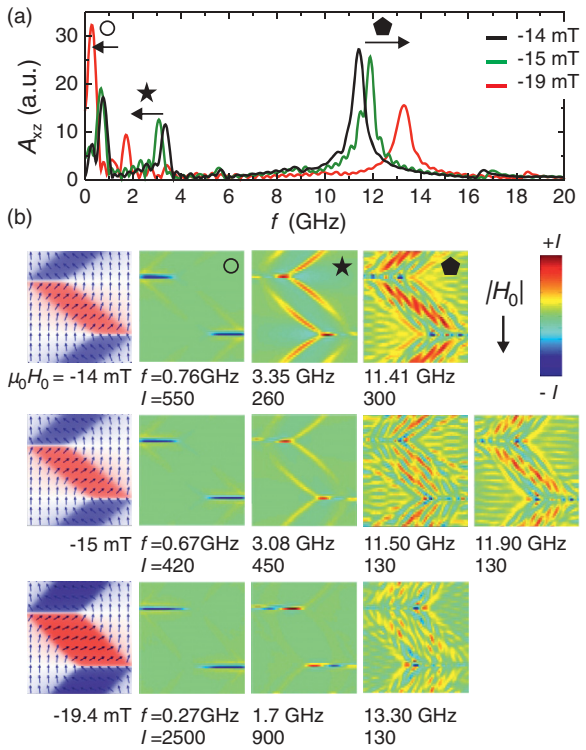

FIG. 4. (Color online) (a) Comparison of the permeability spectra of a buckling pattern with varying negative magnetic fields. Symbols group peaks of similar character but at different applied fields H_0. The change in frequency with increasing negative field is indicated by a (black) arrow for each group. (b) Simulated buckling patterns for different negative fields (left column) and corresponding dynamic snapshots related to the peaks tagged in (a).

found to decrease as the negative field increases. However, the domain mode frequency shows the opposite trend. Increasing the negative field results in a higher domain mode frequency as long as the field is smaller than the switching field ($|H_0| < H_c$). Hence, the numerical results qualitatively reflect the measured FMR data. As exemplarily shown in Fig. 4 for the field of -15 mT, small side peaks close to the main domain mode may appear in the spectra, depending on the applied field strength. One can see from the corresponding mode images at 11.5 and 11.9 GHz that closely spaced domain modes of similar character are excited. Due to the different $f(H_0)$ dispersion, these modes may be resolved as individual peaks or result in one broad domain resonance peak. The excitation of similar domain modes explains the observation of multiple distinct resonance features in the FMR spectra for $0 < H_0 < H_c$.

Again, the domain modes spread over the entire basic and closure domain volume. When the magnetization of the basic domains progressively tilts out of the bar axis with increasing negative field, the degree of inhomogeneity of the dynamic mode in the basic domains increases as well. A dominant modulation parallel to $\vec{M}$ is clearly visible in the basic domain at $\mu_0 H_0 = -14$ mT. Such a mode character is similar to the low-energy magnetostatic spinwave modes found in homogeneously magnetized films, known as backward volume modes.[37] However, at the higher reversal field of $\mu_0 H_0 = -19.5$ mT the amplitude is strongly reduced and a modulation perpendicular to $\vec{M}$ becomes more apparent. Furthermore, it seems that the element geometry is additionally reflected in the mode profile (see the modulation parallel to the element edges).

Before discussing the origin of the resonance increase in the domain mode, we first investigate how the domain modes depend on the buckling wavelength at a fixed static field H_0.

B. Effect of buckling wavelength

Due to the fact that the domain size depends on the simulation geometry and the applied field, it is important to investigate how the wavelength of the buckling state affects the dynamic response. For a given bias field H_0 our numeric simulation results in either a broad (λ_2) or a narrow (λ_1) wavelength buckling pattern depending on the field history [see inset in Fig. 5(a)]. The latter was obtained by decreasing the field from positive saturation to -15 mT. A further decrease in the field to -19.4 mT results in coarsening of the buckling pattern. The coarse configuration is then conserved when the field amplitude is reduced again to -15 mT. In the following we investigate relaxed magnetic domain structures of varying λ at an applied bias field of $H_0 = -15$ mT [see magnetization states in Fig. 5(b)].

Both the domain mode and the wall mode frequencies are strongly affected by the wavelength of the two initial states. Comparing the domain wall mode images for different buckling wavelengths [Fig. 5(b)], a change in the wall mode character becomes obvious. This is related to the different separation of neighbored basic domain walls, i.e., a stronger wall interaction in the case of the λ_1 state. The frequency of comparable wall modes is reduced after coarsening. In contrast, the domain mode frequency increases significantly, from 10.5 to 11.9 GHz after coarsening. Also, for the

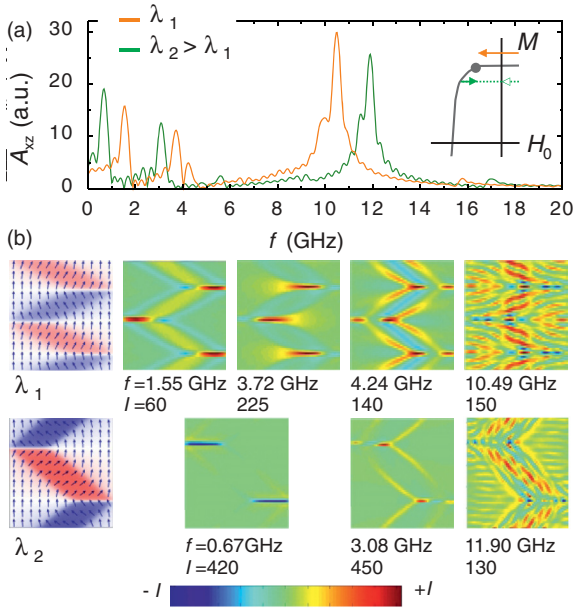

FIG. 5. (Color online) (a) Comparison of permeability spectra of buckling patterns at different wavelengths at a negative field of −15 mT. Inset: Schematic of the demagnetizing branch of a hysteresis curve. Arrows indicate the different field histories. (b) Simulated buckling pattern at short and long wavelength (left columns) and corresponding dynamic snapshots related to the peaks in (a).

short-wavelength buckling state an amplitude modulation parallel to the local magnetization dominates the domain mode character. It seems that such a dynamic modulation can more easily adapt to the smaller change of the magnetization direction across the domain walls, resulting in a more homogeneous mode character. This may be due to the reduced domain wall angle on the one hand. On the other hand, the magnetization inside the smaller closure domains is less homogeneous than in the case of longer wavelengths because the tails of the diagonal Néel walls extend farther into the interior of the closure domains.

IV. DISCUSSION AND CONCLUSIONS

Following the reversal branch of the magnetization curve and increasing the magnetic field, the buckling domain pattern is altered in terms of (i) an increasing magnetization rotation out of the element's long axis inside the basic domains, (ii) an increase in the buckling wavelength within distinct areas, and, finally, (iii) a collapse of the domain pattern and alignment of the magnetization along the field direction. It has been shown experimentally and numerically that case i provokes an increase in the domain mode frequency. Hence, the presence of the buckling domain state for fields $0 < H_0 < 5\,\mathrm{kA/m}$ causes a strong resonance frequency increase, in contrast to the negative dispersion found in Refs. 26–28. There, the magnetization remains uniform and oriented opposite to the reversal field direction before switching due to the different element shapes and material properties.

Our numerical simulations reveal distinct wall modes in the low-frequency range of the dynamic permeability spectra. However, we could not identify well-resolved low-frequency modes in our FMR measurements. Sharp domain wall modes are not expected in the FMR experiment due to the variation in domain wall length (due to the varying element width) and pinning landscape in the lens structures. Hence, various wall modes with closely spaced frequencies will smear and result in one broad peak. The frequency of the FMR low-frequency mode decreases with increasing H_0, which is in accordance with the field-dependent simulations at a constant buckling wavelength. We assume that the origin of the reduction in the wall mode frequency is due to the increasing wall length as H_0 increases. The stiffness of a horizontal domain wall decreases as the distance between the two pinning sites—the intersection point with the diagonal walls on one side and the stripe edge on the other—increases. A lower domain wall stiffness results in a reduction in energy that is associated with a homogeneous oscillation of the wall and thus a lower frequency.[36] Park *et al.*[17] also observed a reduction in the resonance frequency of diagonal walls in a Landau domain pattern when the wall length was increased by a larger element size. The higher order wall modes in our simulation involve larger dipole and exchange energies and thus exhibit a higher frequency the shorter the length of the domain wall. However, it is not trivial to derive the nodal character of the wall modes from simple symmetry arguments in such a buckling domain state. A decrease in the buckling wavelength results in a stronger interaction between neighboring walls and therefore affects the wall mode character.

The domain mode exhibits amplitude modulations parallel and perpendicular to the local magnetization direction inside the center and the edge domains. Thereby, the resonance frequency of the domain mode shows a trend towards increasing with the degree of inhomogeneity of the amplitude modulation. Generally, a modulation of the magnetization parallel to $\vec{M}$ comprises less magnetostatic energy compared to a modulation perpendicular to $\vec{M}$, as the latter involves head-to-head magnetization configurations (similar to the higher energy of Damon-Eshbach spin-wave modes compared to backward volume modes).[37] The same argument holds for static magnetization ripple structures, for which the magnetization is modulated longitudinally along the mean magnetization direction due to a lower stray-field energy being involved.[23] Hence, the more the dynamic modulation deviates from the pure longitudinal ($\|M$) character (in other words, with increasing inhomogeneity), the higher is the measured resonance frequency.

The higher the magnetic field, the stronger is the tilt of the magnetization out of the easy axis and the larger are the domain wall angles. The same is observed for increasing buckling wavelength: When λ increases, the magnetization of the basic domains deviates more strongly from the easy axis and therefore the domain wall angles are increased. Hence, for the cases of the field and wavelength dependence of the buckling state dynamics, we have shown that small domain wall angles between closure and basic domains result in a lower domain mode frequency. When the magnetization changes only slightly across a low-angle domain wall the propagation vector of the dynamic modulation can adapt easily to the change in the magnetization direction [see Fig. 5(b), top row; $f = 10.49$ GHz]. This results in a relatively homogeneous *dynamic charge pattern* in the whole element. In

other words: sinks and sources of the dynamic magnetization are homogeneously distributed, resulting in a lower dynamic magnetostatic energy contribution. Distinct modes that were observed in the FMR spectrum [compare Fig. 2(c)] correspond to similar high-frequency domain modes whose frequency spacing varies with the applied field.

In conclusion, the magnetodynamics of buckling domain states were studied, both experimentally and numerically, by varying the magnetic field amplitude and for different buckling wavelengths. We have shown that the modeled high-frequency domain mode qualitatively explains the measured FMR data of lens-shaped elements in the domain regime for $0 < H_0 < 5\,\mathrm{kA/m}$. Qualitative arguments based on magnetostatic energy considerations were derived to allow for an interpretation of the dynamic response in such low-symmetric magnetization distributions. No well-resolved quantized modes can be expected in buckling domain configurations due to the complex anisotropic and nonmonotonic dipole-exchange dispersion.[21] An increase in the domain wall angles due to magnetization rotation or domain coarsening results in a higher dynamic dipolar potential and therefore in a higher domain mode frequency. After the collapse of the buckling state, the resonance frequency drops back and follows the expected Kittel behavior.

ACKNOWLEDGMENTS

The authors thank R. Mattheis and K. Kirsch (IPHT Jena) for thin-film preparation. We gratefully acknowledge the help of U. Wolff in realizing initial magnetic force microscopy imaging. We also acknowledge the support of M. Dvornik (University of Exeter) in providing useful advice on performing micromagnetic simulations with OOMMF. Finally, we thank M. Wolf for fruitful discussions. Financial support was granted by the Studienstiftung des deutschen Volkes.

*Corresponding author: c.patschureck@ifw-dresden.de
†Current address: Vacuumschmelze GmbH & Co. KG, 63450 Hanau, Germany.

[1] C. Kittel, *Introduction to Solid State Physics*, 7th ed. (John Wiley & Sons, New York, 1996).
[2] S. Jung, J. B. Ketterson, and V. Chandrasekhar, Phys. Rev. B **66**, 132405 (2002).
[3] Z. K. Wang, M. H. Kuok, S. C. Ng, D. J. Lockwood, M. G. Cottam, K. Nielsch, R. B. Wehrspohn, and U. Gösele, Phys. Rev. Lett. **89**, 027201 (2002).
[4] S. O. Demokritov and B. Hillebrands, in *Spin Dynamics in Confined Magnetic Structures I, Topics in Applied Physics, Vol. 87*, edited by B. Hillebrands and K. Ounadjela (Springer, Berlin, 2002), pp. 65–92.
[5] F. Giesen, J. Podbielski, T. Korn, and D. Grundler, J. Appl. Phys. **97**, 10A712 (2005).
[6] V. V. Kruglyak, A. Barman, R. J. Hicken, J. R. Childress, and J. A. Katine, J. Appl. Phys. **97**, 10A706 (2005).
[7] M. Bailleul, R. Höllinger, and C. Fermon, Phys. Rev. B **73**, 104424 (2006).
[8] G. Gubiotti, M. Madami, S. Tacchi, G. Carlotti, A. O. Adeyeye, S. Goolaup, N. Singh, and A. N. Slavin, J. Magn. Magn. Mater. **316**, e338 (2007).
[9] F. Zighem, Y. Roussigné, S. M. Chérif, and P. Moch, J. Phys.: Condens. Matter **19**, 176220 (2007).
[10] B. B. Maranville, R. D. McMichael, S. A. Kim, W. L. Johnson, C. A. Ross, and J. Y. Chen, J. Appl. Phys. **99**, 08C703 (2006).
[11] D. Polder and J. Smit, Rev. Mod. Phys. **25**, 89 (1953).
[12] U. Ebels, L. Buda, K. Ounadjela, and P. E. Wigen, Phys. Rev. B **63**, 174437 (2001).
[13] U. Ebels, L. D. Buda, K. Ounadjela, and P. E. Wigen, in *Spin Dynamics in Confined Magnetic Structures I, Topics in Applied Physics, Vol. 87*, edited by B. Hillebrands and K. Ounadjela (Springer, Berlin, 2002), pp. 167–216, and references therein.
[14] J. Ben Youssef, N. Vukadinovic, D. Billet, and M. Labrune, Phys. Rev. B **69**, 174402 (2004).
[15] S. A. Manuilov, A. M. Grishin, and M. Munakata, J. Appl. Phys. **109**, 083926 (2011).
[16] S.-B. Choe, Y. Acremann, A. Scholl, A. Bauer, A. Doran, J. Stöhr, and H. A. Padmore, Science **304**, 420 (2004).
[17] J. P. Park, P. Eames, D. M. Engebretson, J. Berezovsky, and P. A. Crowell, Phys. Rev. B **67**, 020403 (2003).
[18] K. Perzlmaier, M. Buess, C. H. Back, V. E. Demidov, B. Hillebrands, and S. O. Demokritov, Phys. Rev. Lett. **94**, 057202 (2005).
[19] M. Yan, G. Leaf, H. Kaper, R. Camley, and M. Grimsditch, Phys. Rev. B **73**, 014425 (2006).
[20] U. Queitsch, J. McCord, A. Neudert, R. Schäfer, L. Schultz, K. Rott, and H. Brückl, J. Appl. Phys. **100**, 093911 (2006).
[21] M. Bailleul, R. Höllinger, K. Perzlmaier, and C. Fermon, Phys. Rev. B **76**, 224401 (2007).
[22] H. van den Berg and D. Vatvani, IEEE Trans. Magn. **18**, 880 (1982).
[23] A. Hubert and R. Schäfer, *Magnetic Domains—The Analysis of Magnetic Microstructures*, 3rd ed. (Springer-Verlag, Berlin, 2009).
[24] J. Steiner, R. Schäfer, H. Wieczoreck, J. McCord, and F. Otto, Phys. Rev. B **85**, 104407 (2012).
[25] J. McCord, A. Hubert, G. Schröpfer, and U. Loreit, IEEE Trans. Magn. **32**, 4806 (1996).
[26] J. McCord, R. Mattheis, and D. Elefant, Phys. Rev. B **70**, 094420 (2004).
[27] F. Giesen, J. Podbielski, T. Korn, M. Steiner, A. van Staa, and D. Grundler, Appl. Phys. Lett. **86**, 112510 (2005).
[28] G. de Loubens, A. Riegler, B. Pigeau, F. Lochner, F. Boust, K. Y. Guslienko, H. Hurdequint, L. W. Molenkamp, G. Schmidt, A. N. Slavin, V. S. Tiberkevich, N. Vukadinovic, and O. Klein, Phys. Rev. Lett. **102**, 177602 (2009).
[29] J. M. Garcia, A. Thiaville, J. Miltat, K. J. Kirk, J. N. Chapman, and F. Alouges, Appl. Phys. Lett. **79**, 656 (2001).
[30] A. Hubert, W. Rave, and S. L. Tomlinson, Phys. Status Solidi B **204**, 817 (1997).
[31] C. Bilzer, T. Devolder, P. Crozat, C. Chappert, S. Cardoso, and P. P. Freitas, J. Appl. Phys. **101**, 074505 (2007).
[32] M. Donahue and D. G. Porter, *OOMMF User's Guide, Version 1.0, Interagency Report NISTIR No. 6376* (National

Institute of Standards and Technology, Gaithersburg, MD, 1999); [http://math.nist.gov/oommf].

[33]C. Bilzer, T. Devolder, J.-V. Kim, G. Counil, C. Chappert, S. Cardoso, and P. P. Freitas, J. Appl. Phys. **100**, 053903 (2006).

[34]K. M. Lebecki, M. J. Donahue, and M. W. Gutowski, J. Phys. D **41**, 175005 (2008).

[35]V. A. Ignatchenko, P. D. Kim, T. Y. Mironov, and D. C. Khvan, Sov. Phys. JETP **71**, 331 (1990) [Zh. Eksp. Teor. Fiz. **98**, 593 (1990)].

[36]J. M. Winter, Phys. Rev. **124**, 452 (1961).

[37]A. N. Slavin, S. O. Demokritov, and B. Hillebrands, in *Spin Dynamics in Confined Magnetic Structures I, Topics in Applied Physics, Vol. 87*, edited by B. Hillebrands and K. Ounadjela (Springer, Berlin, 2002), pp. 35–64.